Chapter 3

Spectrum-Sliced WDM Using OOK Transmission

This chapter presents one of the primary contributions of this dissertation: a mathematical model to analyze and evaluate noise-like spectrum-sliced systems which employ conventional PIN receivers, or as proposed in this dissertation, optical preamplifier receivers. As discussed in previous chapters, spectrum-slicing provides a low-cost alternative to the use of multiple coherent lasers for WDM applications by utilizing spectral slices of a single broadband noise source for creating the multichannel system. In this chapter we analyze the performance of both PIN and optical preamplifier receivers for spectrum-sliced WDM using actual noise distributions, and the results are compared with those using the Gaussian approximation. This extends prior results of Marcuse [44,45], for the detection of deterministic signals in the presence of optical amplifier and receiver noise. Although the methodology is similar, the results are considerably different when the signal is itself noise-like. For the case of noise-like signals, it is shown that when an optical preamplifier receiver is used, there exists an optimum filter bandwidth which minimizes the detection sensitivity for a given error probability. Moreover the evaluated detection sensitivity, in photons/bit, represents an order of magnitude (>10 dB) improvement over conventional detection techniques that employ PIN receivers. The Gaussian approximation is shown to be overly conservative when dealing with small ratios of the receiver optical to electrical bandwidth, for both PIN and preamplifier receivers. Finally it is shown how the use of forward error correction (FEC) coding can lead to significant improvement in the transmission capacity of SS-WDM systems.

The chapter is organized as follows. The motivation for this analysis is discussed in Section 3.1. Section 3.2 introduces the basic concepts of the incoherent detection of noise-like signals. An outline of the receiver structure used in the analysis and a detailed discussion of the

mathematical formulation of the problem is contained in Section 3.3. Section 3.4 presents analytical results for the receiver sensitivity of conventional spectrum-sliced systems which employ PIN receivers, and Section 3.5 contains the corresponding results for an optical preamplifier receiver. In both cases, an exact analysis approach, for the idealized case of rectangular spectra, using chi-squared statistics, is compared with the commonly used Gaussian approximation. The analysis and the probability distributions employed are similar to those of Marcuse [44,45]. However, whereas Marcuse considered the case of deterministic signals, we consider the case of noise-like signals, for which the results are considerably different. The chapter is concluded with some system considerations for a preamplifier receiver based SS-WDM. System capacity is calculated with channel bandwidths chosen to maximize power budget. Using the amplified spontaneous emission noise from an optical amplifier as the wideband source, the system capacity (for $P_e = 10^{-12}$) is shown to be 23 Gb/s without coding, and 75 Gb/s with a (255,239) Reed Solomon Code.

3.1 Introduction and Motivation

Experiments with spectrum-sliced WDM (SS-WDM) systems have considered conventional PIN or APD receivers, and performance analysis has generally assumed the Gaussian approximation. To reduce the fluctuations in signal energy it is necessary that the optical bandwidth of the spectrum-sliced signal (B_o) be large compared to the bit rate ($R_b = 1/T$). As $m = B_o T$ is made large, the receiver sensitivity approaches that of a system with a deterministic signal. However, if the optical bandwidth is increased, fewer channels can be supported by the WDM system; moreover a larger optical bandwidth will result in a dispersion penalty. On the other hand, as m is made smaller, signal energy fluctuations result in a power penalty; indeed with the Gaussian approximation, as shown later in this chapter, there is a minimum m necessary to achieve a given error probability.

The purpose of this chapter is two-fold. First, we analyze the sensitivity of a PIN receiver for a spectrum-sliced signal considering the actual distributions of signal and

noise, and show that the Gaussian approximation, although adequate when $m >> 1$, is grossly conservative for small values of *m*. We then consider the case of a receiver utilizing an optical preamplifier. There are now two competing effects; as *m* increases signal energy fluctuations decrease, but amplifier ASE noise increases. There should then be an optimum optical bandwidth to achieve a minimum received number of photons per bit, for a given error probability.

The results that are presented indicate that optically preamplifying the received signal prior to photodetection offers an optimum in terms of the product of the average photons/bit and $m = B_o T$ where B_o is the optical bandwidth per channel of the WDM system and T is the reciprocal bit rate. By operating at this optimum, the system has a larger power budget, which means longer unrepeatered distances, and uses the minimum optical bandwidth/channel, which translates into a larger number of WDM channels in the given noise bandwidth of the broadband incoherent source. Moreover, operation at the optimum ensures that the error probability requirements are maintained.

3.2 Incoherent Detection of Noise-like Signals

The performance of conventional optical fiber-based communication systems is limited by the quality of the transmitter (LED or laser) and the receiver (PIN diode or avalanche photodiode). Ideally the only source of noise in this system is the quantum or shot noise which arises due to the statistical nature of electron-photon conversions at the transmitter and at the receiver. As shown in Section 2.2, the theoretical minimum (quantum-limited) receiver sensitivity is 10 photons/bit. This means that if the receiver were an ideal photon counter, at least 10 photons would be required, on an average, to decide whether the received symbol is a 1 or a 0. Practical systems, however, use less than perfect components and the thermal noise generated by the electronic circuitry in the receiver puts a lower limit on the minimum receiver power. For most practical receivers the receiver sensitivity is at least ten times poorer than the quantum noise limit [1,5].

For the spectrum-sliced WDM system under consideration, the signal source is the amplified spontaneous emission (ASE) noise from a broadband, incoherent optical amplifier. Hence in addition to the thermal noise generated at the receiver, there exists an excess intensity noise term which arises due to the mixing of the similar frequency spontaneous emission components of the optical amplifier source. This noise term, referred to as the spontaneous-spontaneous beat noise, was discussed in detail in Section 2.4. Here it will suffice to say that this excess noise term is dependent on the optical as well as the electrical bandwidth of the receiver. For moderate data rates, for which the optical bandwidth is much larger than the electrical bandwidth, there is negligible degradation in terms of power penalty to the system [13]. If, however, the data rate is increased with the same optical bandwidth, error rate floors are observed. This physically implies that the system is no longer signal power limited, and no amount of increase in signal power (or amplifier gain) can help to reduce the bit error rate. The rapid increase in excess beat noise, which is inversely proportional to the optical bandwidth/channel, places an upper limit on the signal-to-noise performance, and hence the available power budget, of the system. For example a system operating at 1.5 μm with a 0.5 nm filter will experience BER floors at 10^{-8} when the data rate is increased from 2 Mb/s to 1 Gb/s. Such error floors, however, disappear when the optical bandwidth is increased to 1 nm. [13].

The observation, that a high-power superluminescent source has an additional excess photon noise component which dominates SNR performance at high signal powers, was first highlighted by Morkel *et al.* in 1990 [46]. In their experiment, a 7.3 m length of erbium-doped germanosilicate fiber was pumped at 980 nm with approximately 40 mW of pump power from an argon-ion-pumped Styryl-13 dye laser. The signal and noise (fluctuating components) spectra were measured and the noise current plotted against the mean photocurrent. The results for the incoherent broadband source were compared with a similar experiment performed using a coherent He-Ne laser source. The experimental results proved that the noise current from the He-Ne laser was well predicted by the shot-noise theory, and that from the superluminescent source matched with the excess noise theory. Moreover the measured SNR in a unit bandwidth for the coherent source

increased linearly according to the shot noise-based expression -- SNR = $\langle I_s \rangle / 2qB_e$, where $\langle I_s \rangle$ is the mean signal current and B_e is the receiver electrical bandwidth; hence SNR is directly proportional to $\langle I_s \rangle$. The SNR results for the incoherent source, however, did not vary with a change in the detector current being bound by a constant SNR = B_o / B_e where B_o was the optical bandwidth of the source given by

$$B_o = \left[\int P(\nu)d\nu\right]^2 \Big/ \int P^2(\nu)d\nu \qquad (3.1)$$

where $P(\nu)$ is the power spectral density of the optical field as a function of frequency ν.

The incoherent detection of noise-like signals of optical bandwidth B_o may be accomplished by integrating the received power over a time interval *T*, such that $m = B_oT >> 1$. The signal-to-noise ratio (SNR) required for a given error probability (BER) decreases as *m* increases; however an increase in *m* implies an increase in the required signal energy for achieving the same BER. If *m* is sufficiently large, the fluctuation in the received signal will be small compared to the fluctuations caused by the added receiver noise, and the receiver sensitivity will approach that of the deterministic signal case -- typically several thousand photons/bit for practical optical receivers (such as PIN diodes or avalanche photodiodes).

3.3 Receiver Structure and Mathematical Model

The receiver structure assumed in the following analysis is shown in Fig. 3.1. It consists of an optical bandpass filter followed by an ideal square law detector and integrator which measures the energy in the decision interval. For the case of OOK transmission, the energy is compared to a threshold. The analysis of receiver sensitivity follows directly from the distribution of the energy in a Gaussian random process; the optimum threshold which minimizes the error probability depends on the probability distributions of the signal and noise.

The received signal (in units of current) at the input of the decision circuit may be expressed as [37]

$$I = \frac{1}{2T}\int_0^T \left[x^2(t) + y^2(t) + \tilde{x}^2(t) + \tilde{y}^2(t)\right]dt + I_n \qquad (3.2)$$

where $x(t), y(t), \tilde{x}(t)$, and $\tilde{y}(t)$ are independent, identically distributed (i.i.d) baseband Gaussian processes with (optical) bandwidth $B_o/2$, having zero-mean, and each having a variance σ^2 equal to the photocurrent contributed by *each* of the two orthogonal polarizations. Note that the four terms within the integral correspond to two orthogonal phases and two orthogonal polarizations. Also, I_n is the thermal noise current introduced in the electrical portion of the receiver. We neglect shot noise terms since they will be negligible compared to the inherent signal fluctuation noise, and will also be negligible compared to the thermal noise for a PIN receiver, and to the ASE noise for the optical preamplifier receiver.

For the PIN receiver, in the on-state, $x, y, \tilde{x}$, and $\tilde{y}$ are the components of the noise-like signal. These terms are absent in the off-state (*i.e.* perfect extinction assumed). For the optical preamplifier receiver, in the on-state, $x, y, \tilde{x}$, and $\tilde{y}$ are the components of the noise-like signal plus the corresponding components of the preamplifier ASE. In the off-state these are just the components of the preamplifier ASE noise. We assume that the preamplifier gain is sufficiently high that the electrical thermal noise may be neglected. The receiver makes the decision that a 1 was transmitted if $I > I_{th}$ and 0 if $I < I_{th}$, where the optimum threshold (I_{th}) to minimize the error probability is given by

$$P_1(I_{th}) = P_0(I_{th}) \qquad (3.3)$$

where P_1 and P_0 are the probability density functions (pdf) of I for the 1 and 0 states, respectively. The problem then reduces to finding the two pdf's.

Although it is generally difficult to obtain the closed form expression for the distributions, it is relatively straight-forward to obtain their means (μ_1 and μ_0) and standard deviations (σ_1 and σ_0). A common approximation, as discussed in Chapter 2, is then to assume that the distributions are Gaussian in which case the error probability is given by [1]

$$P_e = \frac{1}{\sqrt{2\pi}} \int_Q^\infty \exp(-x^2/2)dx \approx \frac{1}{\sqrt{2\pi}Q} \exp(-Q^2/2) \tag{3.4}$$

where

$$Q = \frac{\mu_1 - \mu_0}{\sigma_1 + \sigma_0}. \tag{3.5}$$

For example Q=6 for $P_e = 10^{-9}$.

The inadequacy of the Gaussian approximation has been treated by Marcuse for the case of deterministic signals. One of the objectives of this chapter is to extend these results to the case of noise-like signals. To obtain the actual distribution of I we need to specify the autocorrelation function (or equivalently the power spectrum) of the baseband Gaussian processes appearing in Eqn. (3.2). For simplicity we assume that these processes have rectangular spectra of bandwidth $B_o/2$, and that the integrals in (3.2) may be approximated by sums in which case

$$I = \frac{1}{2m} \sum_{i=1}^{4m} \left[x_i^2 + y_i^2 + \tilde{x}_i^2 + \tilde{y}_i^2 \right] \tag{3.6}$$

with $m = B_o T$, and where the terms in the summation are independent. Thus the summation is the sum of the squares of $4m$ independent Gaussian variates and is thus chi-square distributed with $4m$ degrees of freedom with the pdf given by [47]

$$P_Y(y) = \frac{(0.5/\sigma^2)^{2m}}{\Gamma(2m)} y^{2m-1} \exp(-y/2\sigma^2) \tag{3.7}$$

where $\Gamma(..)$ represents the standard gamma function. Our objective is to find the pdf which describes the photocurrent I. As expressed in Eqn. (3.6), I is scaled by a factor of $(1/2m)$ appearing in front of the summation sign. Hence defining $X=(1/2m)Y$, the pdf for I may be evaluated as follows.

$$\Pr\{X < x\} = \Pr\left\{\frac{1}{2m} Y < x\right\} = \Pr\{Y < 2mx\} = \int_0^{2mx} P_Y(y)\,dy \tag{3.8}$$

Hence the corresponding pdf for the modified variable X, represented as $P_X(x)$ is given by

$$P_X(x) = \frac{d}{dx}\int_0^{2mx} P_Y(y)\,dy = 2m\Pr(y = 2mx) \tag{3.9}$$

which after some manipulation is represented in the form of a modified chi-square distribution as

$$P_X(x) = P(x) = \frac{(m/\sigma^2)^{2m}}{(2m-1)!} x^{2m-1}\exp(-mx/\sigma^2). \tag{3.10}$$

where the gamma function has been expressed in the form of a factorial. It can easily be verified that Eqn. (3.10) satisfies all the properties of a pdf, such as

$$\int_{-\infty}^{\infty} P_X(x)dx = 1. \tag{3.11}$$

Moreover its various moments are given by

$$\mathrm{E}(X) = \int_{-\infty}^{\infty} x\,P_X(x)dx = 2\sigma^2 \tag{3.12}$$

and

$$\mathrm{E}\left(X^2\right) = \int_{-\infty}^{\infty} x^2\,P_X(x)dx = \left(\frac{\sigma^2}{m}\right)^2\left(4m^2 + 2m\right) \tag{3.13}$$

with

$$\text{var } X = \mathrm{E}\left(X^2\right) - \left[\mathrm{E}(X)\right]^2 = \frac{2}{m}\sigma^4. \tag{3.14}$$

It should be noted that Eqn. (3.10) is consistent with the expression for the probability density function for the spontaneous-spontaneous beat noise derived by Marcuse [44,45] and others [48,49]. Rather than sampling, Marcuse expands the output in a trigonometric series, and assumes that the expansion coefficients are independent. Both approaches are equivalent, and

indeed are equivalent to the classical Karhunen-Loeve expansion [50], with the assumption that there are *m* equal eigenvalues. A discussion of this equivalence is presented in Appendix A. The distribution given in (3.10) is used in later sections to obtain an exact analysis of the performance of a PIN and optical preamplifier receiver, respectively, and the results compared with the Gaussian approximation.

3.4. PIN Receiver Detection for SS-WDM

This section evaluates the receiver sensitivity of conventional SS-WDM systems that employ PIN receivers. The results are of interest in demonstrating the inadequacy of the Gaussian approximation, and are also used later for highlighting the advantage of using an optical preamplifier receiver.

3.4.1 Gaussian Approximation

It follows from (3.2) and (3.6) that the mean and standard deviation of the photocurrent are given by

$$\mu_1 = 2\sigma^2 \qquad \mu_0 = 0 \tag{3.15}$$

$$\sigma_1^2 = (2/m)\sigma^4 + \sigma_g^2 \qquad \sigma_0^2 = \sigma_g^2 \tag{3.16}$$

where σ_g^2 is the variance of the thermal noise current (the subscript *g* denotes Gaussian). Using (3.5) and solving for σ^2 gives

$$\sigma^2 = \frac{\sigma_g Q}{1 - \left(Q^2/2m\right)}. \tag{3.17}$$

Note that σ^2 is the mean signal photocurrent in the on-state in one polarization. Therefore, defining $\overline{N}_p$ as the average number of photons per bit (averaged over on and off states) it follows that

$$\sigma^2 = \overline{N}_p \eta q R_b \tag{3.18}$$

where η is the quantum efficiency of the photodetector and q the electron charge. The variance of the thermal noise current is given by [33]

$$\sigma_g^2 = \left(4V_T q B_e / Z\right) = 8\pi V_T C_T q B_e^2 \tag{3.19}$$

where V_T is the thermal potential (product of Boltzmann's constant and the temperature (300 K) divided by the electronic charge), B_e the receiver electrical bandwidth, Z the effective noise impedance, and C_T the effective noise capacitance of the receiver is related to Z by

$$C_T = \left(1/2\pi Z B_e\right). \tag{3.20}$$

(For example, with C_T = 0.1 pF and B_e = 2.5 GHz, σ_g = 0.255 nA). Substituting (3.18) and (3.19) in (3.17), and using

$$B_e = \left(1/2T\right) = \left(R_b/2\right) \tag{3.21}$$

we obtain

$$\overline{N}_p = \left(\frac{Q}{2\eta}\sqrt{\frac{8\pi C_T V_T}{q}}\right) \Big/ \left(1 - \frac{Q^2}{2m}\right). \tag{3.22}$$

For example, with Q = 6, η = 0.7 and C_T = 0.1pF, it follows that

$$\overline{N}_p = 2732/\left(1 - 18/m\right). \tag{3.23}$$

Hence for a given data rate, the receiver sensitivity is a function of the ratio of the optical to electrical bandwidth per channel of the SS-WDM system. The factor of 18 implies that bit error rate (BER) floors above 10^{-9} will be observed when the $B_o T$ product is reduced to less than 18. Moreover when $m >> 18$, (16) reduces to the deterministic receiver sensitivity value of a few thousand photons/bit (as shown in Section 2.4 of the previous chapter), which is expected. The power penalty resulting from the signal energy fluctuations of the noisy broadband source is given by -10log(1-18/m), so that m must be at least 88 for the penalty to be less than 1 dB.

3.4.2 Exact Analysis

As discussed in Section 2, for simplicity we consider here the case where the integration in the receiver is approximated by a summation and hence results in the received signal being modified

chi-squared distributed with 4*m* degrees of freedom, with the density function given by Eqn. (3.10). The 1 bit is represented by a burst of noise from the source to which post-detection thermal noise is added; the 0 bit is thermal noise alone. The probability density function of the thermal noise component is given by

$$P_g(x) = \frac{1}{\sqrt{2\pi\sigma_g^2}} \exp\left(-x^2/2\sigma_g^2\right). \tag{3.24}$$

Since the signal is chi-squared distributed and the thermal noise is Gaussian, the signal+noise term at the decision circuit is given by the convolution of the modified chi-squared and the Gaussian distributions. The convolution yields the following expression for the resultant distribution

$$\begin{aligned} P_r(x) &= P(x) * P_g(x) \\ &= \frac{K}{(2m-1)!}\alpha^m \int_0^\infty \exp[-(a\xi^2 + b\xi + c)]d\xi \end{aligned} \tag{3.25}$$

where

$$K = 1/\sqrt{2\pi\sigma_g^2}\,, \tag{3.26}$$

$$a = 1/2\sigma_g^2 = 1/2(8\pi V_T C_T B_e^2) \tag{3.27}$$

$$b = m\alpha - 2ax \tag{3.28}$$

where

$$\alpha = 1/\sigma^2 = 1/\overline{N}_p \eta q R_b \tag{3.29}$$

and

$$c = ax^2. \tag{3.30}$$

Using a standard mathematical software (Mathematica), the closed form expression for Eqn. (3.25) was evaluated to be

$$P_r(x) = \frac{K}{(2m-1)!}(m\alpha)^{2m}\frac{a^{-(1+2m)/2}}{2\exp(c)}\left[\sqrt{a}\,\Gamma(m)\mathrm{Hyg}(m,0.5,b^2/4a) - b\,\Gamma(0.5+m)\mathrm{Hyg}(0.5+m,1.5,b^2/4a)\right] \tag{3.31}$$

where 'Hyg' refers to the Kummer confluent hypergeometric function and Γ is the gamma function [51] . This extends the results of a recent paper by Nguyen *et al.* [52] which although

considering the PIN receiver for the case of spectrally sliced signals, assumes that the distribution of signal plus noise may itself be approximated by a modified chi-square. We believe that our approach, outlined above, is a better approximation since we employ a more exact (Gaussian + chi-square) distribution for the photocurrent at the decision circuit.

The optimal decision threshold $x = x_{th}$ occurs at the intersection of the distribution functions associated with the 1 and the 0 bits. Assuming equiprobable 1 and 0 bits, the resultant error probability is then

$$P_e = 0.5\left[\int_{-\infty}^{x_{th}} P_r(x)dx + \int_{x_{th}}^{\infty} P_g(x)dx\right]. \tag{3.32}$$

The choice of a threshold that minimizes the error probability is given by $P_r(x_{th}) = P_g(x_{th})$. A sub-optimal choice of the threshold, but one that is very close to the optimum when the error probabilities are very small, is to chose x_{th} such that the two integrals in Eqn. (3.32) are equal. We make that choice here which then gives

$$P_e \approx \int_{x_{th}}^{\infty} P_g(x)dx. \tag{3.33}$$

Therefore for a 10^{-9} error probability $x_{th} = 6\sigma_g$. Using this relation in (3.31), and simplifying using (3.27) and (3.28) with C_T = 0.1pF and η = 0.7 as before, we obtain the desired relationship between the receiver sensitivity and m as

$$\frac{0.5}{(2m-1)!}\left(\frac{644m}{\overline{N}_p}\right)^{2m}\left[\Gamma(m)\mathrm{Hyg}(m,0.5,k) - \left(\frac{644m}{\overline{N}_p}\right)^{-8.5}\Gamma(0.5+m)\mathrm{Hyg}(0.5+m,1.5,k)\right] = 1 \tag{3.34}$$

where

$$k = \frac{103684.58m^2}{\overline{N}_p^2} - \frac{2732.26m}{\overline{N}_p} + 18. \tag{3.35}$$

This is solved numerically and the results ($\overline{N}_p$ vs m) are plotted in Fig. 3.2. (Due to the numerical difficulties in evaluating the hypergeometric terms, the results are calculated only for $m \le 46$.)

Two important points may be readily noted from Fig. 3.2 which graphs the variation in receiver sensitivity as a function of *m* for both the exact analysis and the Gaussian approximation (Eqn. (3.27)). First, a large number of photons/bit (on the order of 10^4), and hence high optical power, is required to maintain the 10^{-9} error probability when *m* is less than about 10. This puts an upper limit on the power budget available for both long-haul and local access SS-WDM systems. Secondly, the Gaussian approximation grossly misrepresents receiver sensitivity at low values of $m = B_o T$, and as expected is very conservative. For example, at $m = 20$ the exact calculation gives a receiver sensitivity that is 7.2 dB better than that of the Gaussian approximation; this difference, however, reduces to 0.8 dB when *m* increases to 45.

Nguyen *et al* [52], who use an approximation for the actual distribution, overestimate the difference between the actual and Gaussian approximations, and results mentioned in their paper predict a difference of almost 16 dB even when *m* is as high as 42. Our theoretical results are generally consistent with simulation of receiver performance recently reported [53]. However, the only system experiment results with which we are familiar [20,21] are for large values of *m* for which the Gaussian approximation is valid. Experiments at lower values of *m* would indeed be of interest.

3.5 Optical Preamplifier Receiver for SS-WDM

In the case of the optical preamplifier receiver, the received photocurrent is given by Eqn. (3.6) (the thermal noise term may be neglected if the amplifier gain is sufficiently large) with now

$$\sigma^2 = \sigma_s^2 + \sigma_n^2 \tag{3.36}$$

in the on-state, and

$$\sigma^2 = \sigma_n^2 \tag{3.37}$$

in the off-state, where

$$\sigma_s^2 = \overline{N}_p \eta q R_b G \tag{3.38}$$

and

$$\sigma_n^2 = n_{sp} \eta q (G-1) B_o \tag{3.39}$$

with n_{sp} and G being the spontaneous emission factor and gain of the optical preamplifier, respectively. Note that for G>>1

$$\frac{\sigma_s^2}{\sigma_n^2} = \frac{\overline{N}_p}{n_{sp}} \frac{R_b}{B_o} = \frac{\overline{N}_p}{m n_{sp}}. \tag{3.40}$$

3.5.1 Gaussian Approximation

It now follows that the means and variances of the photocurrent are given by (see (3.15) and (3.16))

$$\mu_1 = 2\left(\sigma_s^2 + \sigma_n^2\right) \qquad \mu_0 = 2\sigma_n^2 \tag{3.41}$$

$$\sigma_1^2 = \frac{2}{m}\left(\sigma_s^2 + \sigma_n^2\right)^2 \qquad \sigma_0^2 = \frac{2}{m}\left(\sigma_n^2\right)^2. \tag{3.42}$$

From (3.5), and (3.40), (3.41), (3.42), it follows that (assuming G >> 1)

$$\overline{N}_p = \frac{2 n_{sp} m}{\left(\frac{\sqrt{2m}}{Q} - 1\right)}. \tag{3.43}$$

Thus with the Gaussian approximation, there is a minimum *m* given by $Q^2/2$ ($m_{\min}$=18 for Q=6, same as for the PIN receiver). The sensitivity of the receiver, using the Gaussian approximation, is plotted as the dashed curve in Fig. 3.3 for Q = 6 and n_{sp} = 2.

3.5.2 Exact (Chi-square) Analysis

Assuming as above that the preamplifier ASE noise dominates over thermal noise, the photocurrent I for both the 1 and 0 bits are modified chi-square distributed, according to Eqn. (3.10). The error probability assuming equiprobable 1 and 0 bit transmission may be written as [47]

$$P_e = 0.5\left[\Pr\{x > x_{th} \mid 0\} + \Pr\{x < x_{th} \mid 1\}\right] \tag{3.44}$$

where x_{th} is the decision threshold which may be evaluated by recognizing that the probability density functions for the 1 and 0 bits are equal at the threshold. That is

$$\frac{(m/\sigma_1^2)^{2m}}{(2m-1)!}\, x_{th}^{2m-1} \exp(-mx_{th}/\sigma_1^2) = \frac{(m/\sigma_0^2)^{2m}}{(2m-1)!}\, x_{th}^{2m-1} \exp(-mx_{th}/\sigma_0^2) \tag{3.45}$$

where $\sigma_{1(0)}^2$ is the mean photocurrent during the 1(0) bit. Hence the signal threshold may be written as

$$x_{th} = \frac{4\sigma_1^2\sigma_0^2}{\sigma_1^2 - \sigma_0^2} \ln(\sigma_1/\sigma_0). \tag{3.46}$$

Using (3.40) and (3.42), the error probability may be expressed as

$$P_e = \frac{0.5m^{2m}}{(2m-1)!}\left[\int_{K_1\sigma_0^2}^{\infty} \frac{x^{2m-1}}{\sigma_0^{4m}} \exp(-mx/\sigma_0^2)\,dx + \int_0^{K_2\sigma_1^2} \frac{x^{2m-1}}{\sigma_1^{4m}} \exp(-mx/\sigma_1^2)\,dx\right] \tag{3.47}$$

where

$$K_1 = \frac{2}{u}(1+u)\ln(1+u), \tag{3.48}$$

and

$$K_2 = \frac{2}{u}\ln(1+u). \tag{3.49}$$

with

$$u = \left[(\sigma_1^2/\sigma_0^2) - 1\right]. \tag{3.50}$$

If the variable of integration in the first integral is changed to $p = x/\sigma_0^2$ and to $p = x/\sigma_1^2$ in the second integral, then by using the property of probability density functions,

$$P_e = \frac{0.5}{(2m-1)!}\left[\int_0^{\infty} p^{2m-1}\exp(-p)\,dp - \int_0^{mK_1} p^{2m-1}\exp(-p)\,dp + \int_0^{mK_2} p^{2m-1}\exp(-p)\,dp\right]. \tag{3.51}$$

These integrals may be readily evaluated using the incomplete gamma function defined as [54]

$$\Phi(K,p) = \frac{1}{\Gamma(p)}\int_0^K t^{p-1}\exp(-t)\,dt. \tag{3.52}$$

Using the above definitions, the error probability reduces to

$$P_e = 0.5\left[1 - \Phi(mK_1, 2m) + \Phi(mK_2, 2m)\right]. \tag{3.53}$$

It follows from (3.39), (3.41) and (3.49), that

$$u = \overline{N}_p / n_{sp} m \tag{3.54}$$

and consequently K_1 and K_2, are functions of both $\overline{N}_p$ and $m = B_o T$. Equation (3.53) thus provides an implicit relation between $\overline{N}_p$ and m. This is evaluated numerically and the results are plotted as the solid curve in Fig. 3.3 (again for $P_e = 10^{-9}$ and $n_{sp} = 2$).

Thus **Fig. 3.3 shows the comparison of the receiver sensitivity as a function of *m*, for both the exact analysis and the Gaussian approximation. The important observations here are that a) an optimum value of *m* exists corresponding to the minimum value of the receiver sensitivity, b) the sensitivity at the minimum, as shown in Fig. 3.4 in photons/bit, is at least 10 dB lower than that achieved by conventional PIN receivers, and c) the Gaussian approximation again proves to be overly conservative, particularly at low values of *m*.** The optimum value of m and the corresponding receiver sensitivity were evaluated for different error probabilities and the results are shown in Fig. 3.5. It is seen that both the optimum m and the minimum sensitivity vary essentially linearly with $\log P_e$. To express these results in terms of more familiar parameters, Fig. 3.6 shows the optimum bandwidth of the receiver optical bandpass filter as a function of the data rate per channel, at different error probabilities. As shown by the graph, the range of filter bandwidths required to operate at the optimum is between 0.2 to 3.5 nm, for per channel data rates ranging from 1 to 10 Gb/s. The optimum system parameters when a preamplifier is used are hence well within practical limits.

3.6 System Considerations

The above analysis may be used to estimate answers to the following questions: for a given source

noise bandwidth, what is the total transmission capacity at the optimum value of *m*, and what is the power budget that is available when the optical preamplifier receiver is used ?

3.6.1 System Transmission Capacity

We define the transmission capacity T_{cap} of the SS-WDM system as [21]

$$T_{cap} = NR_b = \frac{B_{SS}}{MB_o} R_b = \frac{B_{SS}}{mM} \tag{3.55}$$

where N is the total number of channels in the system, B_{SS} is the available gain bandwidth of the spectrum-sliced source, and M is the ratio of the channel spacing to the optical bandwidth B_o. Using the optimum value of *m* and assuming $B_{SS} = 25$ nm and $M = 3$, Eqn. (3.55) is evaluated for different error probabilities. The results are plotted in Fig. 3.7 and indicate that spectrum-sliced OOK with an optical preamplifier offers a transmission capacity of ~32 Gb/s at $P_e = 10^{-9}$. The assumption of $M = 3$ is, of course, arbitrary, but (we feel) conservative, since the spectrum sliced system, at the optimum bandwidth, is operating at a much lower optical signal-to-noise ratio than that for deterministic signals. (The signal-to-noise ratio at the decision circuit is increased by the post-detection integration). Thus, we expect the spectrum-sliced system to be less sensitive to interchannel interference than that of deterministic systems *having narrower optical bandwidth, but the same ratio of channel spacing to bandwidth.* This, of course, requires experimental confirmation with realistic filter shapes, considering both the effects of the filters on the signal and the noise.

3.6.2 System Power Budget

The available power budget is given by the difference of the transmitted power (in dBm) and the required receiver sensitivity. If a system designer were to use the analysis developed in this chapter, he would select a data rate, and then tune the receiver optical bandwidth to minimize the required minimum received power. Hence power budget in this section is defined in terms of the receiver

optical bandwidth (in nm), assuming a data rate per channel of 2.5 Gb/s, and a power spectral density of 4 mW/nm [23] for the spectrum-sliced source.

Using the parameters quoted above, the transmitted power per channel is given by the product of the PSD and the channel optical bandwidth, and thus in logarithmic units

$$\text{Transmitted Power (dBm)} = 10\left[\log_{10}(4) + \log_{10}(B_{o,nm})\right] \tag{3.56}$$

where $B_{o,nm}$ is the receiver optical bandwidth in nm. Also, at the receiver

$$\begin{aligned}\text{Receiver Sensitivity (dBm)} &= \overline{N}_p h\nu R_b \text{ (in dBm units)} \\ &= 10\log_{10}\left(\overline{N}_p\right) - 94.95\end{aligned} \tag{3.57}$$

Hence using the above equations, the available power budget may be easily evaluated to be

$$\text{Power Budget (dB)} = 100.97 + 10\log_{10}(B_{o,nm} / \overline{N}_p) \tag{3.58}$$

A comparison of the power budget for the PIN and the preamplifier receiver case is shown in Fig. 3.8. As pointed out earlier and as shown in the figure, the preamplifier receiver offers at least a 10 dB improvement in system power efficiency. The figure shows that as the optical bandwidth of the channel is increased, the power budget increases. This is because the increase in optical bandwidth brings about an increase in the transmitted power, as shown in Eq. (3.56). However increase in optical bandwidth also introduces an increasing amount of ASE in the system, which means a higher number of photons are now required to maintain the error probability. This explains the difference in the slope of the power budget curve (Fig. 3.8), for small and large values of the optical bandwidth.

3.7 Use of FEC Coding to Improve Transmission Capacity

Figure 3.5 indicates that the optimum m and the minimum $\bar{N}_p$ both decrease significantly as P_e increases, *i.e.* the total transmission capacity is a strong function of the channel error rate. This suggests that it may be possible to achieve larger power budgets and greater system capacities by operating at relatively high raw bit-error-probability and using forward error-correcting (FEC)

codes. This is shown conceptually in Fig. 3.9 which illustrates the well known concept of trading transmission bandwidth for reduced optical power requirements, in the context of spectrum-sliced transmission.

Figure 3.10 shows the corresponding improvement in transmission capacity as a function of the coding gain, for different code rates. Coding gain, as defined in this chapter, is the ratio of the coded to the uncoded P_e, for the case when the coded $P_e = 10^{-12}$. As the coding gain increases, the optimum value of m decreases because the uncoded P_e increases, but this is partially negated because the effective bit duration is longer than the binary symbol duration. The latter factor is small for long high-rate codes. For example, for randomly distributed bit errors, a (255,239) Reed-Solomon code can correct P_e of $P_e = 10^{-4}$ to a P_e of better than $P_e = 10^{-12}$ [55]. This corresponds to coding gain of 10^8 and code rate of 0.94. As shown by the **X** in Fig. 3.10, a transmission capacity of the order of 75 Gb/s is achievable with this rate code.

The receiver sensitivity also changes due to the incorporation of FEC coding. However, the ratio of the (coded) filter bandwidth to the receiver sensitivity (in photons/bit) stays relatively constant (for high rate codes), and following Eqn. (3.58), there is no significant change in the system power budget. Thus, FEC allows significant increases in system capacity without degrading the power budget, or alternatively larger power budgets may be achieved at a given capacity by utilizing narrower system bandwidths [56].

3.8 Discussion

To summarize, we have shown that an optical preamplifier receiver for spectrum-sliced OOK-based WDM systems results in considerably improved receiver sensitivity compared to conventional spectrum-sliced systems employing p-i-n receivers. Moreover it has also been shown that the Gaussian approximation is useful only when operating with large ratios of the receiver optical to electrical bandwidth. We calculated the resulting transmission capacity and power budget and proposed the use of FEC coding to improve transmission capacity in such systems. The theoretical models used in this evaluation [57,58] do not assume the Gaussian approximation, but do assume

ideal rectangular filter shapes. Although increased transmitter power, and/or noise cancellation techniques [59] are alternatives to the use of optical preamplifiers in spectrum-sliced WDM systems, it is (we feel) still important to understand the performance that can be achieved with optical preamplifiers. Furthermore, the results presented may be readily extended to the case of long-distance networks in which intermediate optical amplifiers are employed as linear repeaters. Even though experiments to verify these results remain to be done, the results are sufficiently promising to indicate that spectrally-sliced systems with optical preamplifier receivers may be an encouraging technique for both local-access and long-haul applications.

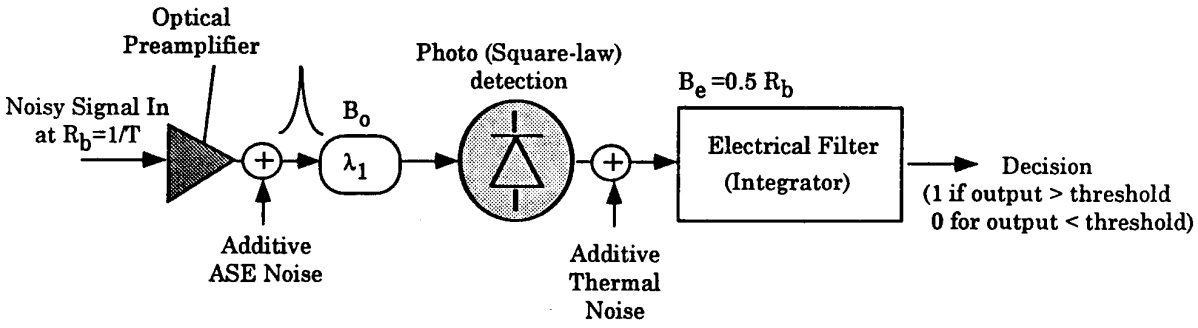

Fig. 3.1: *On-Off Keying (OOK) receiver model.*

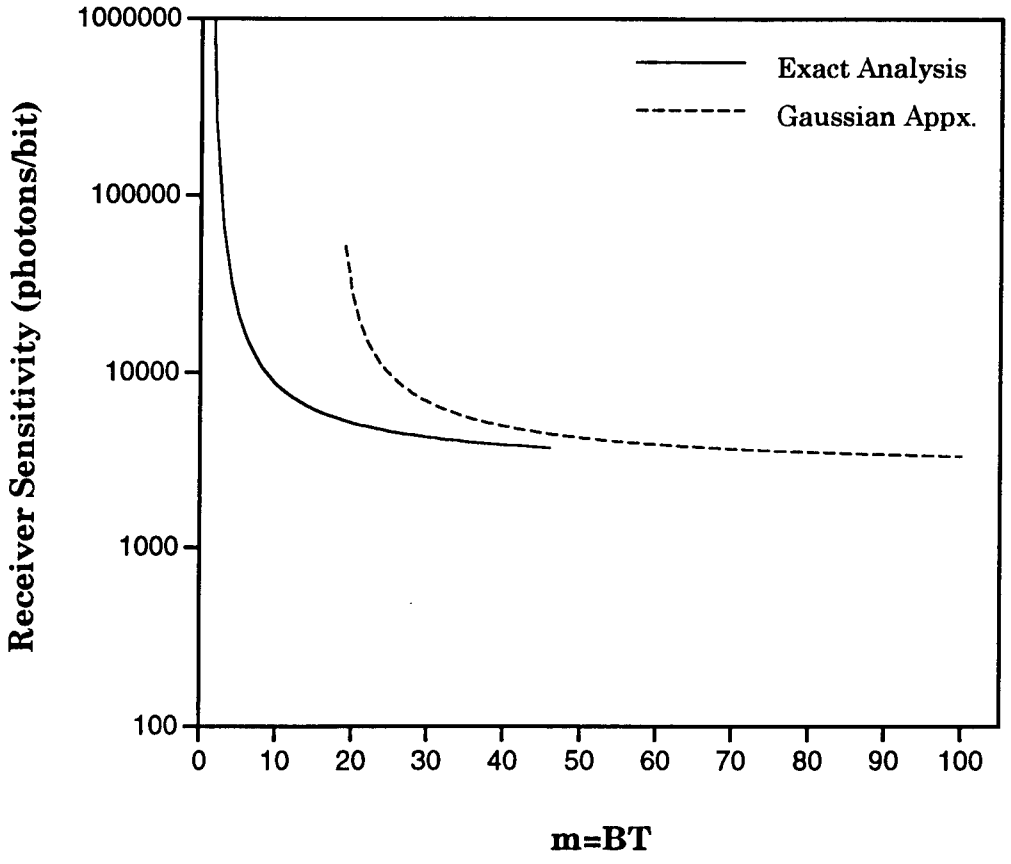

Fig. 3.2: *Receiver sensitivity at* $P_e = 10^{-9}$ *for PIN (*$C_T = 0.1\text{pF}$, $\eta = 0.7$ *), as calculated with the exact and Gaussian distributions.*

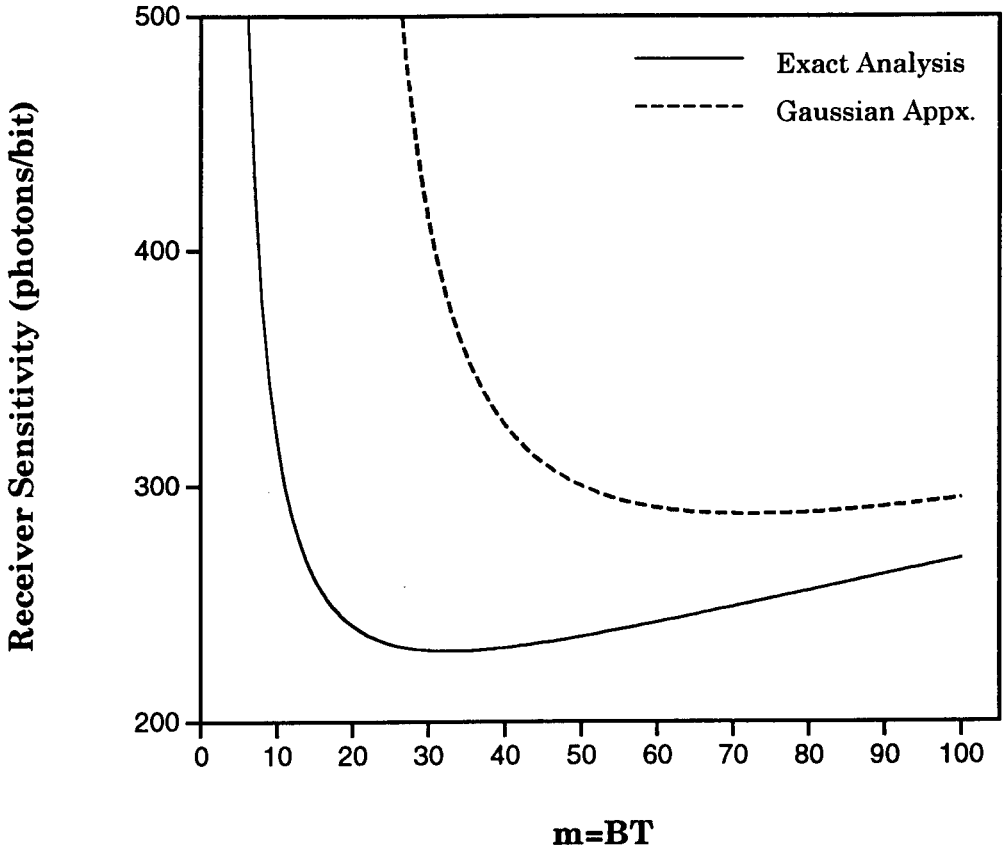

Fig. 3.3: *Receiver sensitivity at* $P_e = 10^{-9}$ *for an optical preamplifier receiver (*$n_{sp} = 2$*) as calculated with the exact and Gaussian distributions.*

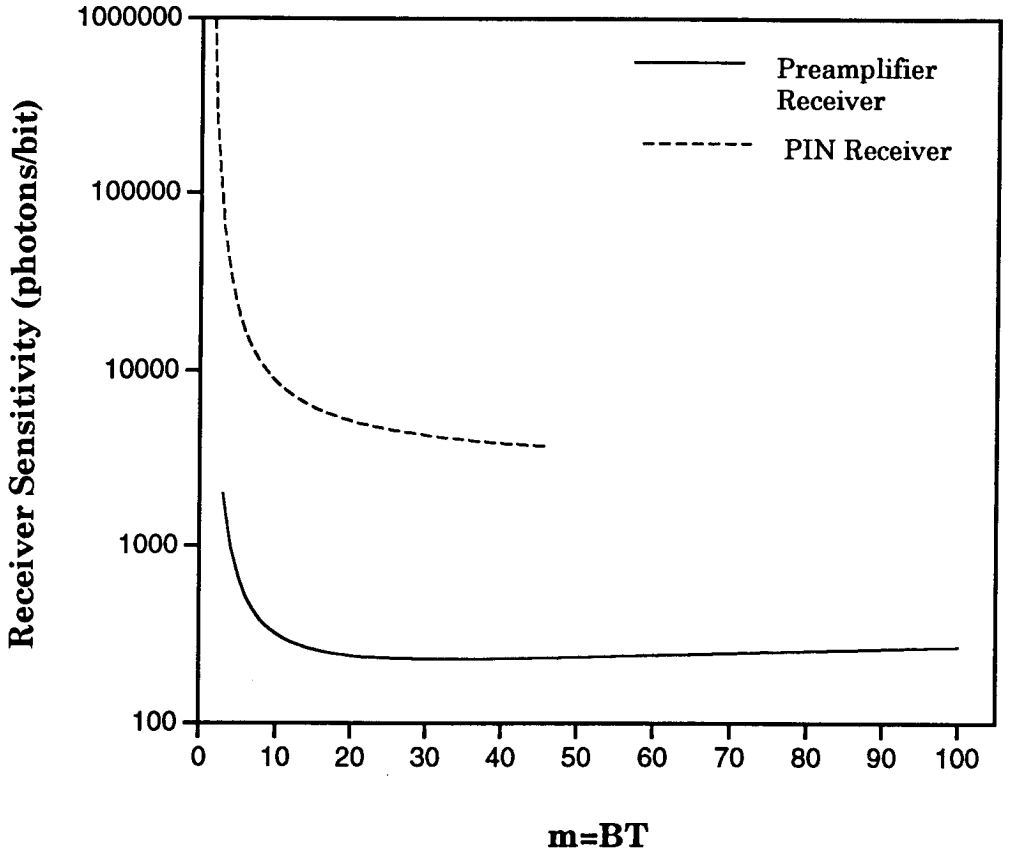

Fig. 3.4: *Receiver sensitivity comparison for a PIN ($C_T = 0.1$pF, $\eta = 0.7$) and a preamplifier receiver ($n_{sp} = 2$) for a SS-WDM system.*

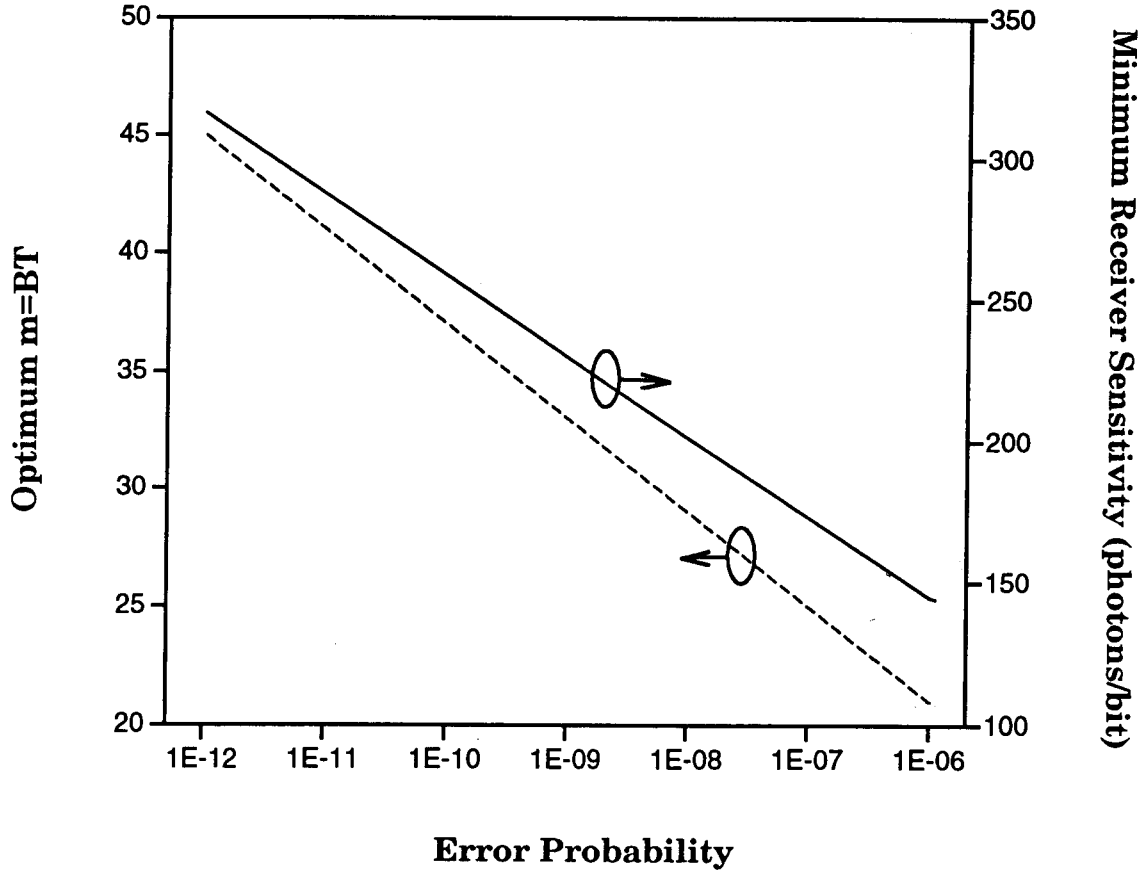

Fig. 3.5: *Optimum $m = B_oT$ and the corresponding minimum average receiver sensitivity $\overline{N}_p$ (in photons/bit), evaluated at different error probabilities.*

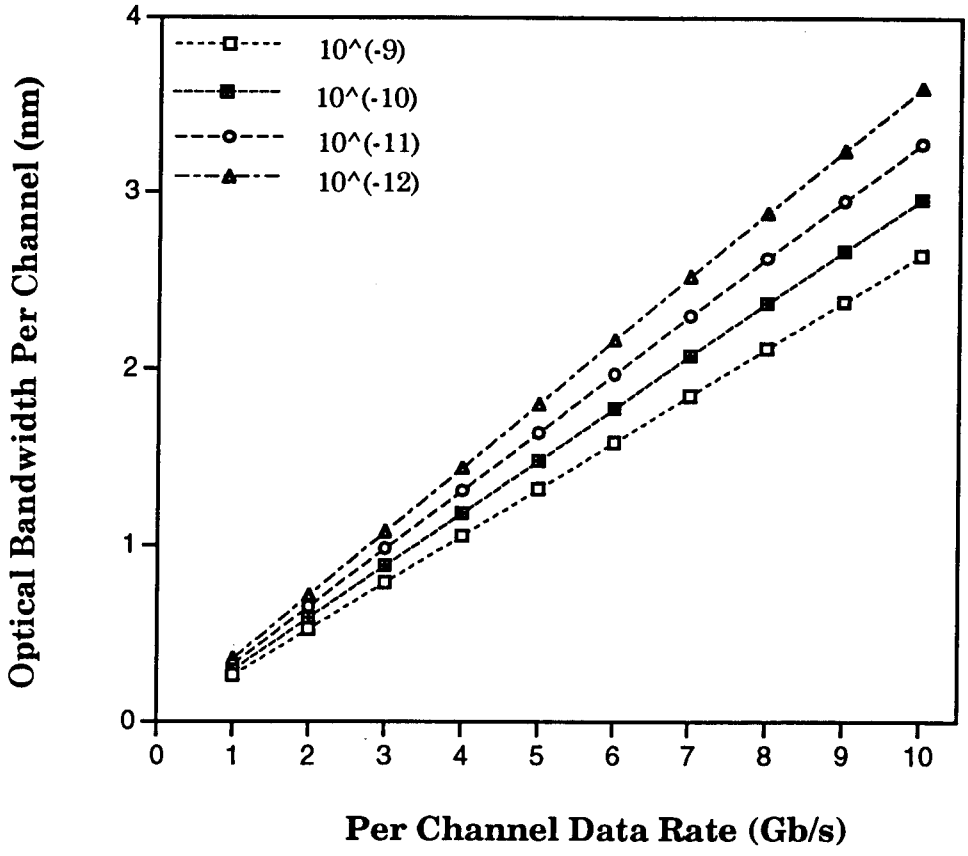

Fig. 3.6: *Optimum filter bandwidths predicted by the exact analysis for the preamplifier case, evaluated as a function of per channel data rates, at various error probabilities.*

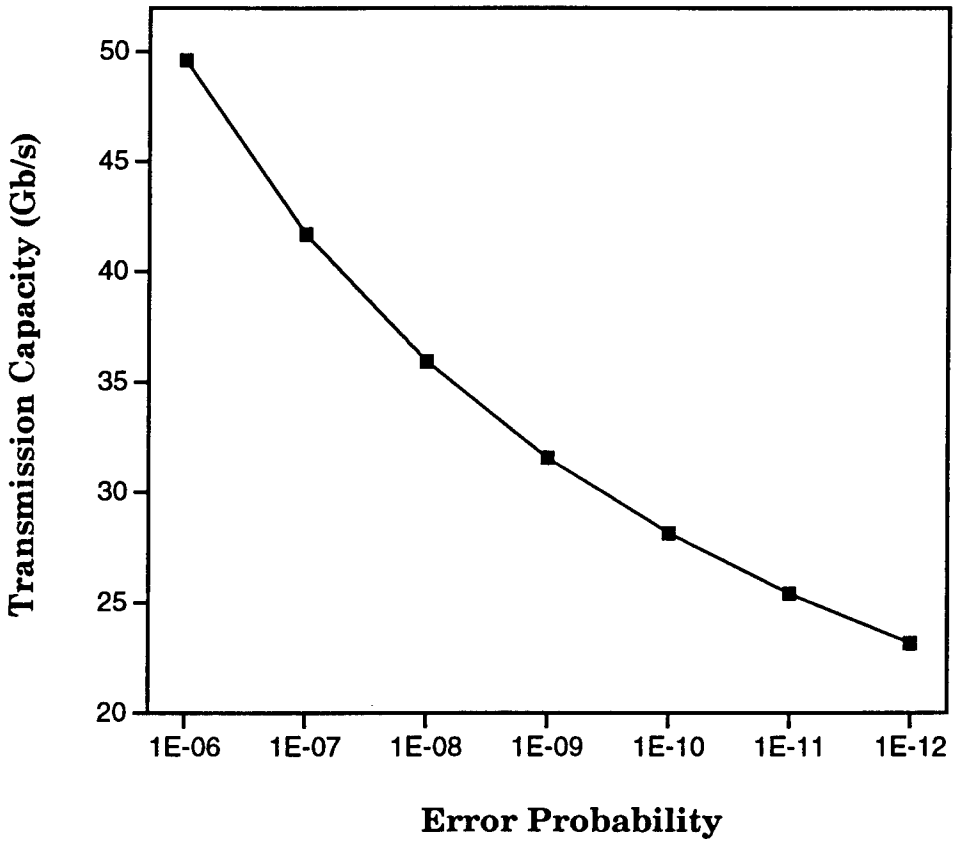

Fig. 3.7: *Predicted transmission capacity in Gb/s for an optical preamplifier receiver-based SS-WDM system, operating at the optimum.*

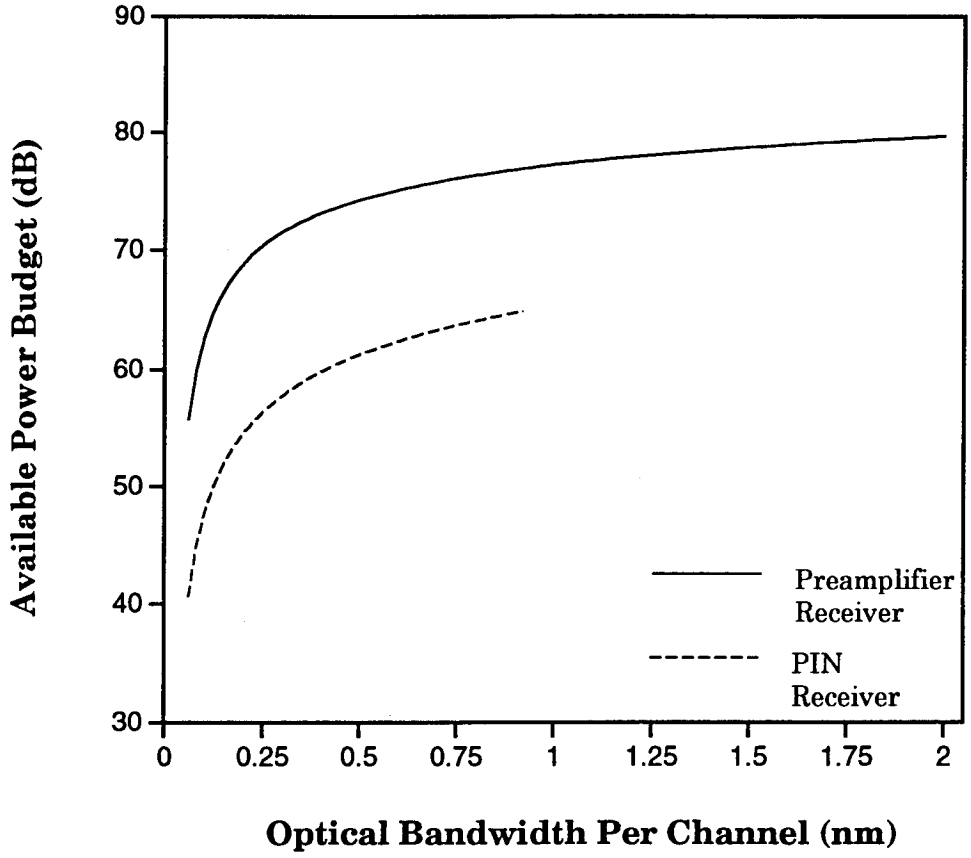

Fig. 3.8: *Available power budget as a function of the optical bandpass filter bandwidth for the optical preamplifier receiver, assuming the power spectral density of the spectrum-sliced source to be 4 mW/nm and a 2.5 Gb/s per channel data rate.*

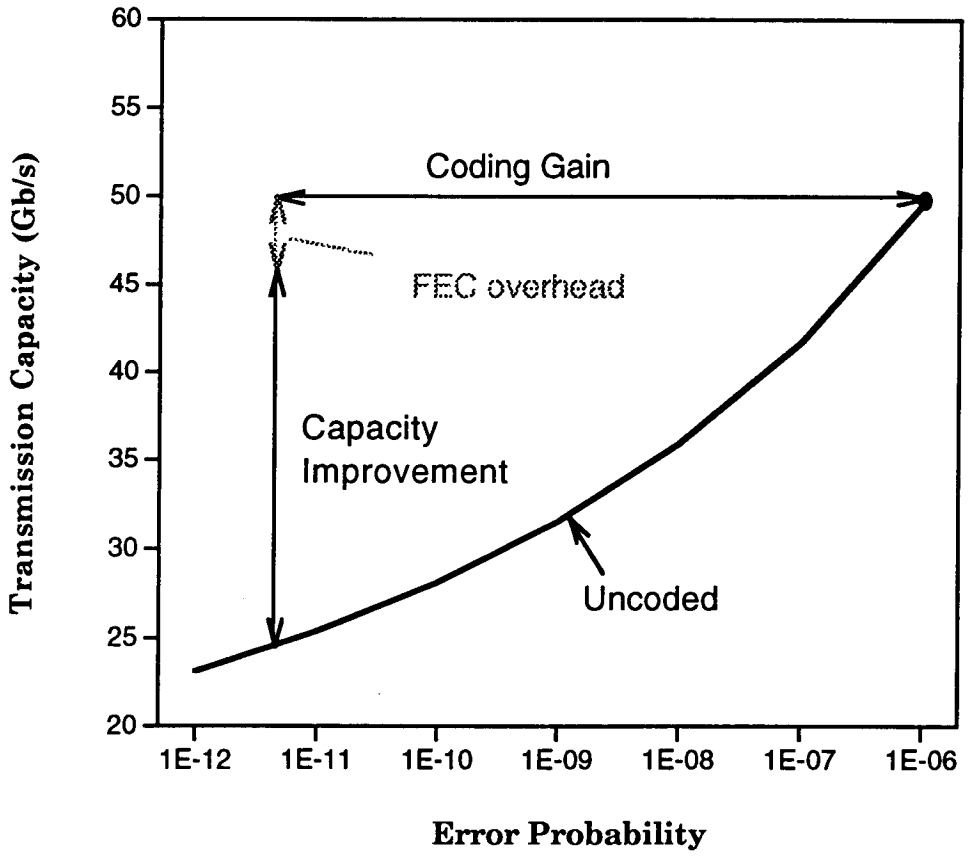

Fig. 3.9: *Motivation for FEC coding.*

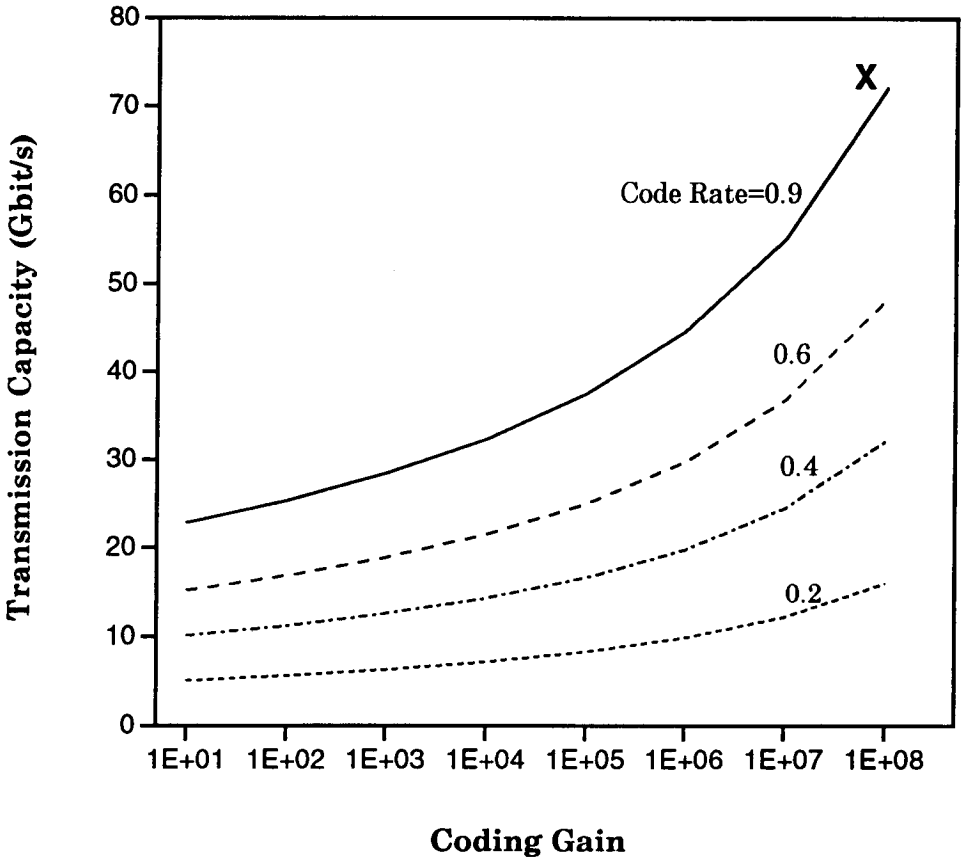

Fig. 3.10: *Transmission capacity (in Gb/s) versus coding gain for different code rates.*